This is a repository copy of *Investigating Al-Si base abradable material removal mechanism with axial movement in labyrinth seal system*.

White Rose Research Online URL for this paper:
https://eprints.whiterose.ac.uk/190804/

Version: Published Version

Article:
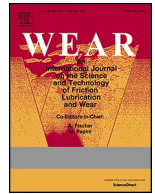
Investigating Al-Si base abradable material removal mechanism with axial movement in labyrinth seal system

Boxiu Zhang [*], Matthew Marshall, Roger Lewis

Department of Mechanical Engineering, Sir Frederick Mappin Building, Mappin Street, Sheffield, UK

ABSTRACT

Modern aeroengines employ labyrinth seal systems to seal the clearance between the blade tip and surrounding engine casing. Understanding of the wear mechanism between labyrinth fins and abradable coatings on the casing is necessary to help the aeroengine achieve higher efficiency. In this study, multiple tests with different types of fin geometries are conducted on a high-speed test rig with a fin tip speed of 100m/s. Two motorized stages are used to simulate the axial movement of the labyrinth fin in an aeroengine. The wear mechanism is investigated over a range of incursion rates from 2μm/pass to 10μm/pass, with in-situ force and temperature measurements along with high-speed imaging recorded on the side in each case. The surface examination of the wear track is also employed by using microscopy post-test. The main abradable material removal mechanism is extruding from the fin side. Also, adhesion of abradable material to the fin is found in each test and the adhesion amount is affected by both fin geometry and incursion rate.

1. Introduction

Previous studies conducted into the material removal mechanism present in a radial fin / abradable liner seal, used at various points of an aero-engine, have focused on radial incursion events [1-4]. In some cases, this contact has been investigated by considering a single short fin segment incurring into an abradable sample, whereas in others a fully circumferential fin has been utilised. In all of these studies, displacement of material as opposed to fracture has been identified as the dominant material removal mechanism, representing a markedly different material removal regime to that seen for interactions between compressor or turbine blades and abradable liners. Recently, the influence of fin geometry on the material removal mechanism was also investigated, where it was determined that whilst the arc length of the fin did indeed change the wear process, material displacement was still the dominant mechanism.

As noted, fins are used at various stages of the engine in combination with abradable liners to create seals. Common examples include on the shaft as a continuous circumferential ring, or where they are mounted as individual segments onto the end of turbine blades forming a continuous circumferential seal in concomitance. Whilst previous testing of fin seal systems has focused on radial incursion events, axial motion of the fin into the abradable is also a frequent occurrence. Such events happen as a

consequence of changing axial airflow rates, leading to the turbine disc assembly moving in the axial direction. Similarly, in the event of bearing cross overs as a consequence of forces developed during specific flight manoeuvres, axial motion of the turbine is again developed, leading to axial fin seal incursion events. In this latter case, engine data suggests that a typical turbine fin can move at a rate of 1.5mm/s, or the equivalent of 10 microns per revolution considering the test rig used to investigate fin seals previously [1]. Fig 1 shows an example of a fin seal contact subject to axial motion, where the fin first moves radially into the liner, following a path investigated in multiple previous studies [1,5, 6], before progressing in the axial direction. In this latter case (Fig 1c), the fin makes contact with the side of the groove generated by the radial incursion, resulting in significantly different contact mechanics to that investigated previously.

Previous research on the material removal mechanism in the fin – abradable contact, focusing on radial incursion events, has identified extrusion of the abradable material as the dominant wear mechanism [2], along with a limited amount of compacted material either peeling away from the rub track or rebounding behind the contact [1]. Additionally, a more recent study focused on the role of fin geometry (a single discrete fin, a fin segment and a circular continuous fin), and highlighted that it influenced the severity of the wear event [6]. Given the changes in wear demonstrated with the changes in fin geometry, it is therefore
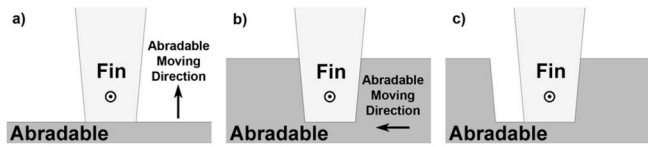
Fig. 1. Fin axial movement a) vertical incursion, b) axial incursion and c) end of axial incursion

likely that the axial incursion generates a further change in behaviour, given that the contact is no longer occurring on the fin tip. Compared to the radial incursion, the fin-abradable contact area is much larger during axial incursion events. Additionally, due to the fin section geometry, the point at which contact stresses occus is now on the side, with orientation of the resultant force also broadly aligned with the incursion direction. As such, exploring material removal in axial rubs is of interest, not least given their relatively frequent occurrence in aero-engines, in order to understand the contribution of axial motion to overall fin wear and hence sealing efficiency.

In order to investigate axial incursion events, a new motorised microscope stage and a purpose built stage holder were used to create axial movement on an existing abradables test platform [7]. The tests were conducted using the procedure as previously detailed for investigating discrete fin samples [1], with the addition of a high frame rate camera at the side of the test rig to investigate extrusion of material from the worn groove during the rub event. By analysing the forces and temperatures developed during the rub, as well as the fin and abradable profile changes, along with inspection of the worn samples post-test, the abradable material removal mechanism of the fin with axial movement was investigated.

2. Methodology

2.1. Test rig

The test rig used in this study was developed from the original incursion test rig proposed by Stringer [7]. Fin samples are mounted within a disc, which is driven by a high speed grinding spindle (GMN HSP-120g, GMN Paul Müller Industrie GmbH & Co. KG, Nürnberg, Germany). In its simplest arrangement, a single active fin is mounted within the disc in order to perform a test, with a shorter dummy fin included 180 degrees opposed to the test fin for balancing purposes. The

maximum operating speed of the spindle is 21000RPM, meaning the test arrangement has a maximum blade tip speed of $200ms^{-1}$. The motion of the abradable sample is controlled by a single axis motorised microscope stage (OSMS80-20ZF-0B, Sigma Koki Co. Ltd., Tokyo, Japan). The microscope stage moves up and down to simulate the radial incursion process and operates between 0.1 and 2000 µms-1, in order to control the test incursion rate from 0.02µm/pass to 2µm/pass. Another single-axis motorised microscope stage (OSMS20-35(X), Sigma Koki Co. Ltd., Tokyo, Japan) was added to the test arrangement in order to facilitate axial movement, enabling axial incursion rates between 1 to 12µm/pass with a total movement range of 35mm to be achieved. Both of the motorised microscope stages are controlled by a dual-channel stage controller (SHOT-202, Sigma Koki Co. Ltd., Tokyo, Japan). The stage controller has two individual channels, so that the two microscope stages can be controlled individually in order to simulate an axial incursion event. It should also be noted that at present, due to limits in the stage controller software, only one stage can move at a given time.

A schematic diagram of the sensor system on the test rig is shown in Fig 2. As shown, the instrumentation includes an image capture system containing a CCD camera (Basler acA1600-60gm, Basler AG, Ahrensburg, Germany) focused on the abradable sample surface during a test (Fig 3), with the aim of identifying extrusion of material from the contact. In order to improve the quality of the images recorded, the camera uses a stroboscopic approach [8] with an LED array mounted opposed to the camera and triggered using a light gate. As shown in Fig 2, the light gate is interrupted by a metal arm mounted on the end of the rotating disc, and once triggered results in the LED emitting a short duration-high
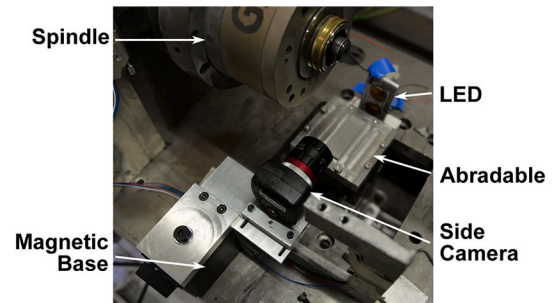
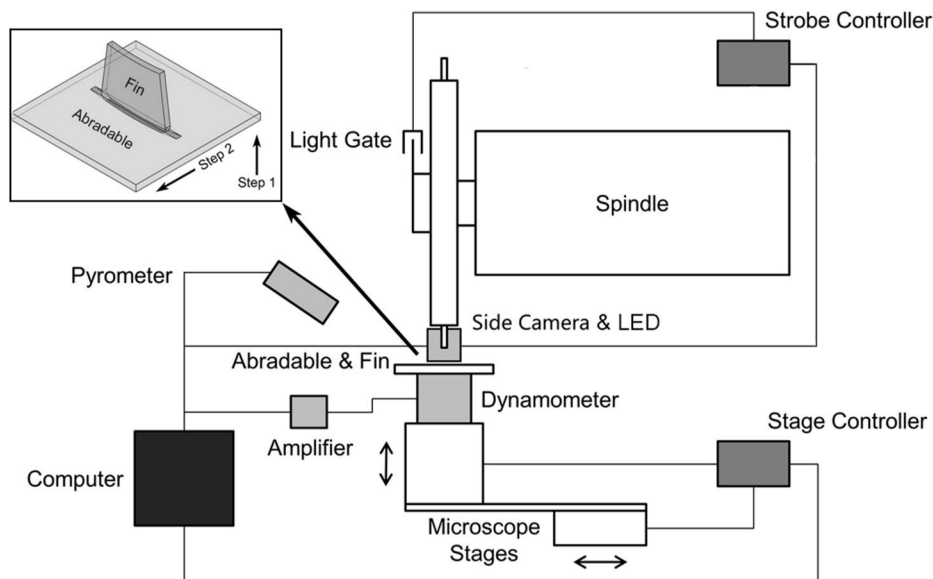

Fig. 3. Arrangement of side camera and LED

Fig. 2. Schematic diagrams of equipment used for an axial movement test

energy pulse in order to illuminate the rub track. A strobe controller sits between the light gate and LED, providing the appropriate power to the LED, as well allowing a delay to be added in order to accurately time the pulse. The CCD camera records three to four exposures per image, with the composite image aligned as a consequence of the stroboscopic approach. Additionally, a web camera is also included in the imaging system in order to monitor the rub, and visually capture if any sparks are emitted from the contact. Aside from the image capture system, the test set-up also includes instrumentation to measure forces and temperatures as a consequence of the incursion event. As the Figure shows, a three axis dynamometer is mounted underneath the abradable sample (Type 9327C, Kistler Instruments Ltd., London, UK), and is capable of measuring forces in the range of ±4kN. Raw signals from the dynamometer are then passed to the control computer via a charge amplifier (Type 5070A, Kistler Instruments Ltd., London, UK), where all measurements made during the incursion event are recorded on a common time base using a purpose built Labiew Vi (Labview, National Instruments, Newbury, UK). Finally, the temperature of the rub is measured using a pyrometer (Thermometer CTLaser M3, Micro-epsilon, Koenigbacher, Germany) focused on the abradable at the contact point between the fin and abradable, in the middle of the arc of contact.

2.2. Test samples

Fig. 4a-c show the three different fin shapes used in this study. As shown, the fins used to consist of a fin segment with a 95mm radius that is joined together with three others to form a complete ring, a fin segment that is used in a pair and a single discrete fin. These fins are similar to those used in a previous study to investigate contact geometry [6]. Fig. 5 shows each of the fin geometries mounted within their respective test discs. As shown, when two segments are used, they are mounted 180 degrees opposed for balancing, resulting in two fin contacts with the abradable per revolution, each 90 degrees in arc length. It should also be noted that the single discrete fin has a radius of 90mm, and is thus matched to the curvature of the disc within which it is mounted. In all cases the fin samples were manufactured from stainless steel (type 304).

Fig. 4d shows the abradable material used in this study. The abradable used is Metco™ 601NS (labelled as M601NS in this paper) with an R15Y hardness of 79-82, when measured using a Rockwell Superficial Hardness Tester. M601NS is an aluminium silicon polymer (AlSi-Polymer) abradable and is produced by plasma sparaying a powder of polyester particles which have been blended with AlSi particles, in this case at a rate of 60g/min. It is typically used with titanium alloy, nickel alloy and steel blades at low temperatures (up to 325°C) [9], and the datasheet provided by the manufacturer [10] suggests the M601NS has high abradability, high oxidation resistance and thermal shock

resistance up to 345°C. As detailed in the figure, the abradable material is thermally sprayed onto a square steel plate to a nominal thickness of 3mm.

As noted, stainless steel has been used as the fin material in this study, and its selection for use against an aluminium-silicon based abradable such as M601NS is relatively uncommon. Indeed, M601NS is typically used in conjunction with titanium alloy-based fins in low-temperature aero-engine applications, where titanium is used to save weight given it has sufficient material properties at such temperatures to achieve a good working performance. However, as noted in previous studies into fin geometry, titanium fins also tend to experience thermal wear [1], with this influencing the material removal mechanism from the abradable. As such, stainless steel has been chosen for the fins in this case given its higher thermal conductivity [11,12], in order to primarily focus on the mechanism through which the abradable breaks down based on the axial incursion event, with future testing planned with alternative fin materials, once the method of abradable material release is identified.

2.3. Test procedure and test parameters

All incursion tests conducted in this study were undertaken following the same test procedure. After attaching the fin and abradable to the test rig, a datum was established by touching the fin onto the top of the abradable sample, and the abradable was then retracted a distance of 500 microns. With the sample retracted, the test was then controlled using the Labview software, whereby the spindle and instrumentation equipment is first initiated, and with the spindle at the programmed test speed, the abradable then incurred into the fin using the stage. In the case of the axial incursion tests presented in this study, there are two movements of the stage assembly in a given test. Firstly, the fin radially incurs into the abradable, before a second movement takes place in the axial direction.

Tests were performed at a blade tip speed of 100m/s, with this speed chosen as it has previously been identified that engine representative wear mechanisms occur in this case, and it is also suitable for accurately imaging the material removal from the abradable [6]. In all cases the radial incursion was performed at a speed of 310μm/s, with this representing an incursion rate of 2μm/pass for the single fin, and reflective of rates seen in running and handling of the engine, where axial events such as bearing crossovers also occur.

As previously mentioned, the maximum anticipated axial movement rate from a bearing crossover event is approximately 10μm/pass, when quantified in the context of this test rig with a single discrete fin employed. Therefore, a series of tests were performed for each fin type at varying axial incursion conditions up to the maximum identified. For the single fin this range was 2-10 μm/pass, which converted into incursion
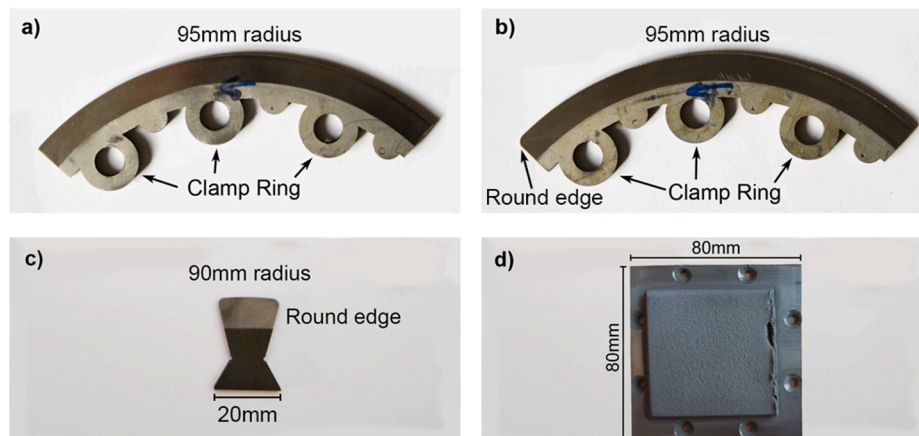

Fig. 4. Three different fin samples, a) whole-ring fin, b) segmental fin, c) single discrete fin and d) abradable
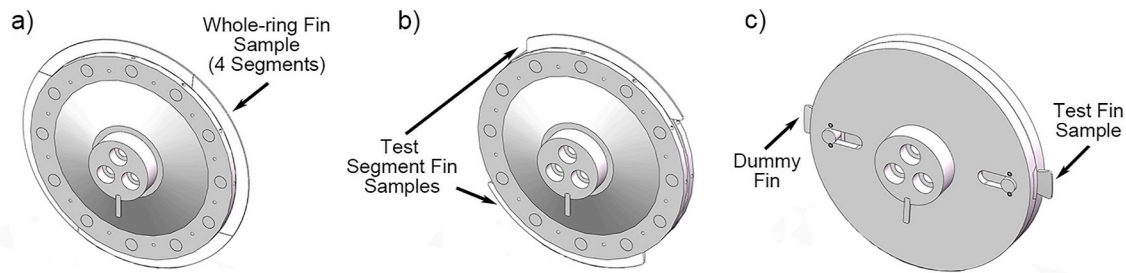
Fig. 5. a) whole-ring fin disc, b) Segment fin disc and c) discrete fin disc used in this study

speeds of 310, 620, 930, 1240, 1550μm/s, which were used in all tests (Table 1). Each test was repeated four times, and average measurements of wear, force, and temperature established in each case. Post-test, fin samples were imaged, and in the case of fin segments subsequently re-used. In this latter case, fin segments were first inspected for damaged, and then refurbished to remove any adhesions prior to re-use. If damage was determined, the fin segment was replaced.

3. Results

In this section the results from the various incursion tests are detailed. This includes post-test inspection of the fin and abradable samples, processed data for contact force and temperature measured during the incursion, and stroboscopic imaging of the abradable material being removed from the rub track. Force and temperature results were post-processed as previously detailed [1], with results plotted for a given test as a function of time. Whilst typically in-situ force and temperature measurements are plotted against cumulative rub length, reflecting the work done by the fin seal, in this instance time was used given the varying levels of circumferential engagement of the different fin designs, as well as the fact the same amount of material was removed in each case.

3.1. Abradable and fin samples post-test

The inspection of abradable and fin post-test provides a direct measure of the wear experienced by the respective bodies in contact. Fig. 6 shows the abradable and fin samples post-test, where for the fin segments the imaging is focused on regions of interest where wear occurred. Specifically, in the fin images the leading edge is on the left hand side of the image, and the top surface as shown, is the surface that makes contact with the abradable during the axial incursion event. It should also be noted, that in Fig. 6 the fin is moving from left to right with rotation across the surface of the abradable sample, and from the

top to the bottom during axial movement.

Fig. 6a-e show the abradable and fin post-test for all tests undertaken using a single discrete fin. As shown in the figures, the abradable material adheres onto the face of the fin for all of the axial incursion rates investigated. Fig. 7 shows an enlarged image of the fin from the test at an axial incursion rate of 620μm/s, where it can be observed that the adhered material is concentrated on the leading and trailing edges of the fin, with more limited evidence of adhesion in the centre of the fin. This coverage was found to progress with axial incursion rate, and indeed for the test performed at 1240μm/s, adhesion was found to be present all the way across the face of the fin. The images of the wear scar on the abradable in Fig. 6a-e, also show a variation in the groove width and length. As shown by the figures, for the single fin the wear scar decreases in width and length with axial incursion rate, following the trend of changes in adhesion with incursion rate seen for the fin. As described in the previous study [1], the groove length is dependent on the maximum fin length during the incursion, with the reduction witnessed as a consequence of fin wear. Similarly, the groove width is dependent on the surface of the fin and the adhesion or wear that occurs on it, with the reduction in width observed with axial incursion rate, indicative of adhesion and wear via the mechanism detailed. In order to further characterise the observed changes in groove width with axial incursion rate, the average width of the wear scar on the samples was measured. As shown by Fig. 8a, the groove width is greater than the expected value in all cases as a consequence of adhesion, with the value dropping with axial incursion rate, where the expected value has been calculated using the fin geometry (thickness) combined with its axial distance of travel.

Fig. 6f-j show the abradable and one of the fin segments, from the tests performed with two fin segments 180 degrees opposed. As noted, the images of the fin samples are focused on areas of interest, where either thermal damage or adhesion could be observed. As the figures show, whilst adhesion is still evident, it is patchy when compared to the single fins discussed previously, and has a more limited correlation with axial incursion rate. One result of particular interest to note is shown in

Table 1
Test matrix for axial movement test

| Fin Shape	Tip Speed [m/s]	Radial Incursion Speed [μm/s]	Radial Incursion Depth [μm]	Axial Incursion Speed [μm/s]	Axial Incursion Depth [μm]
Single discrete	100	310	2000	310	2000
Single discrete	100	310	2000	620	2000
Single discrete	100	310	2000	930	2000
Single discrete	100	310	2000	1240	2000
Single discrete	100	310	2000	1550	2000
Segment	100	310	2000	310	2000
Segment	100	310	2000	620	2000
Segment	100	310	2000	930	2000
Segment	100	310	2000	1240	2000
Segment	100	310	2000	1550	2000
Whole-ring	100	310	2000	310	2000
Whole-ring	100	310	2000	620	2000
Whole-ring	100	310	2000	930	2000
Whole-ring	100	310	2000	1240	2000
Whole-ring	100	310	2000	1550	2000
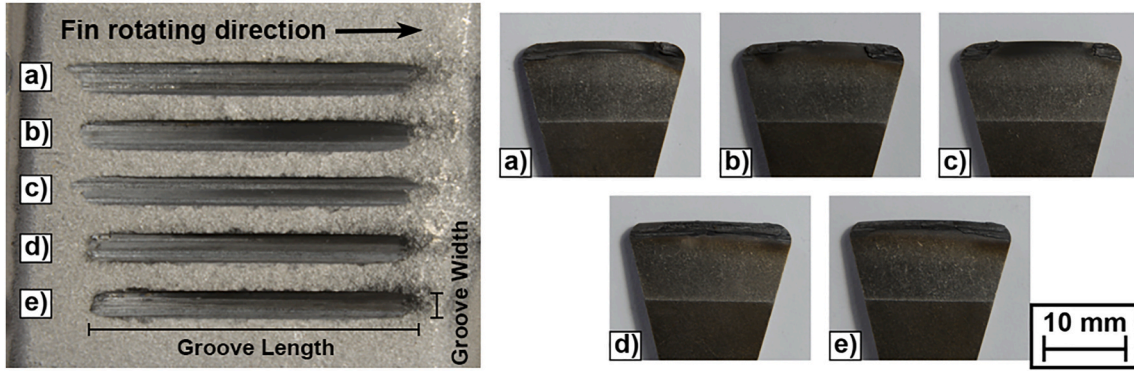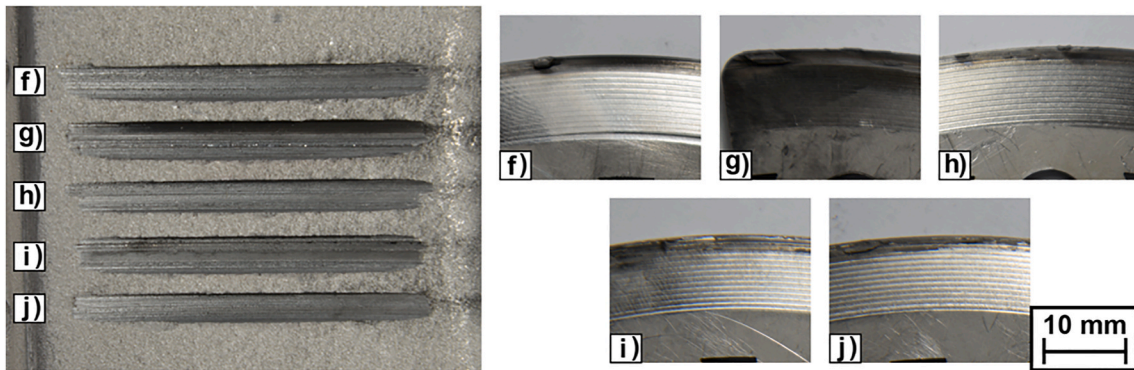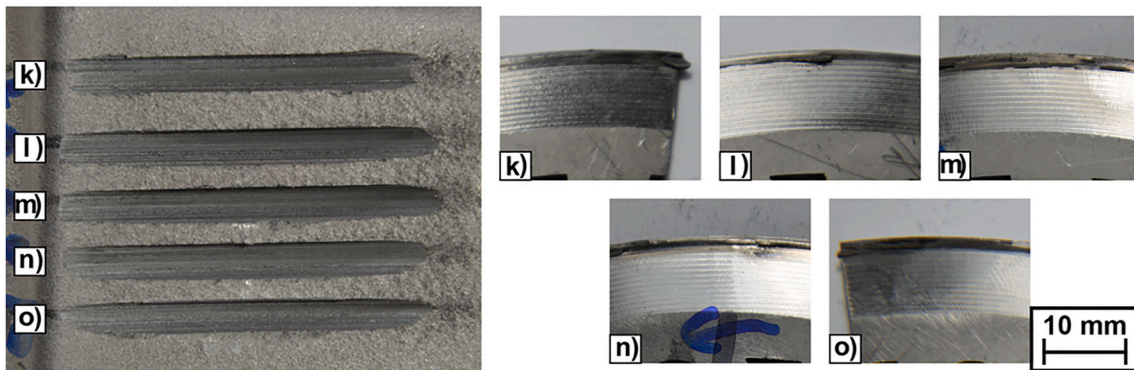
Fig. 6. Abradable and fin profile after test, single discrete fin with axial incursion speed of a) 310μm/s, b) 620μm/s, c) 930μm/s, d) 1240μm/s and e) 1550μm/s; segment fin with axial incursion speed of f) 310μm/s, g) 620μm/s, h) 930μm/s, i) 1240μm/s and j) 1550μm/s and whole-ring fin with axial incursion speed of k) 310μm/s, l) 620μm/s, m) 930μm/s, n) 1240μm/s and o) 1550μm/s

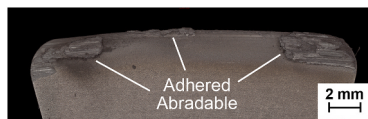**Fig. 7.** Enlarged fin tip of test single discrete fin, 620μm/s

Fig. 6g, for an axial incursion rate of 620μm/s. As the image of the sample shows, thermal damage occurs on both the fin and in the wear track on the abradable, with this damage evident on the abradable approximately half way through the test, as indicated by the marked discolouration of the sample. This result appears to be an anomaly, as thermal damage does not occur to a similar degree on either the preceding or subsequent tests or on any of the other repeat tests at this condition, and will be investigated further in the following sections.

Fig. 8b shows the measured wear scar width for the tests with the fin

segment. As shown in the Figure, adhesion once again influences the wear scar, with significant levels of overcutting occurring for almost all axial incursion rates investigated, and indeed typically to a higher level than that seen for a single fin test at a comparable incursion condition. As noted, the width of the wear scars whilst still correlated with incursion conditions, shows increased variability test to test, with the widest scar occurring for the test at 620μm/s, once gain though, the shortest scar does occur at the highest axial incursion rate investigated. This result suggests that with the fin segments, adhesion is still likely linked to incursion rate, but at the same time is also more transient, leading to the variation in wear scars seen. Finally, this view is also supported by inspection of the samples, where multiple sites of broken off adhesions are evident (Fig. 6).

Finally, Fig. 6k-o show the abradables and fin segments for the tests where four fins are combined to form a single continuous fin around the circumference of the test disc. Measurement of the width of the wear
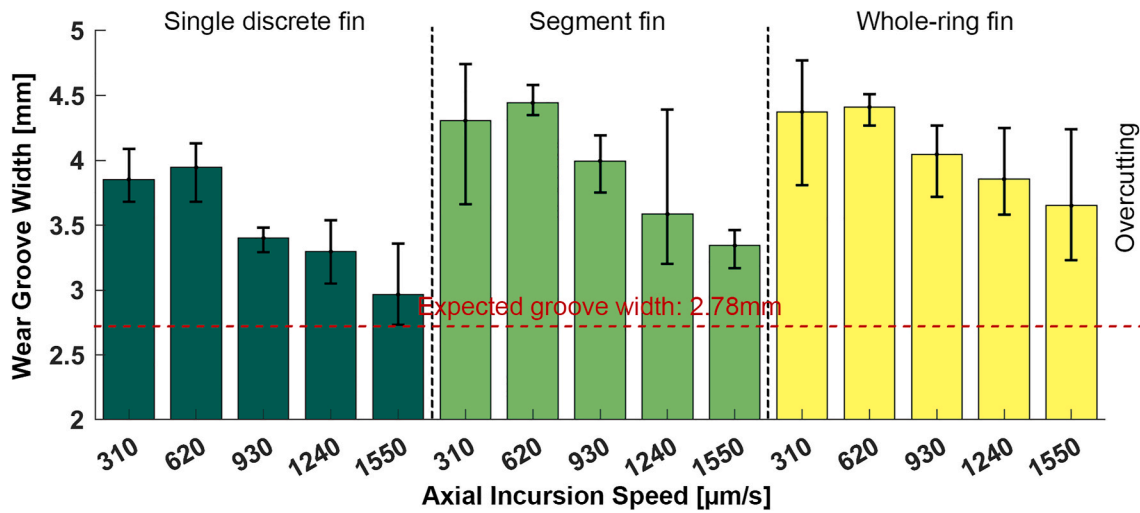
Fig. 8. Wear groove width for tests with single discrete fin, segment fin and whole-ring fin

scar on the abradable are similarly shown in Fig. 8c. As shown in Fig. 6k-o, adhesion is once again evident on the surface of the fin sample, with a reduction in groove width occurring once again with axial incursion rate, although at a reduced rate. This fact is evident when comparing the width of the wear scars shown in Fig. 8c, where the bar chart is flatter when compared to the other fin types. As was previously seen when two fin segments were tested, adhesion has led to wider wear scars than seen for the single fin segment, but variation between conditions is now reduced.

3.2. Force and temperature

In this section the force and temperature measurements recorded during the incursion events are detailed. As discussed previously, forces are measured in three directions, radial to the contact in the direction of the vertical incursion, tangential to the contact following the rotary path of the fin, and finally axial in the direction of the axial incursion. Axial forces are not reported for the vertical incursion, as they fluctuate rapidly in this case as the tapered fin interacts with the abradable material. As shown in the schematic diagram in Fig. 9a, along with the corresponding example force trace (Fig. 9b), as the fin vertically incurs, axial force components are developed on both faces of the fin. Whilst these might be expected to balance, resulting in zero net force, the reality is these forces vary rapidly, as do the other force components, depending on adhesion to the fin, and extrusion of material from the contact [1]. As such, these results are not included, as they are prone to significant fluctuation, and for the current time scale of measurement

have no practical significance. Conversely, a single direction axial force component occurs during the axial incursion event, and values are reported. Since axial force is not reported in vertical incursion and all test condition are the same between each test during vertical incursion, all three force components are presented only during the axial incursion.

Fig. 10 shows the force and temperature measurements for the test with the single discrete fin, where the radial incursion ends after approximately seven seconds, and the axial incursion then begins. Whilst the primary focus of this study is on the forces and temperatures developed in the axial component of the rub, it is also worth noting that values are within the expected range for the radial component of the incursion [1], and subject to the variation typically seen in abradable material – seal fin interactions. Going back to the axial component of the incursion, as the processed results in Fig. 10 show, axial and radial forces are largest and similar in value, followed by lower tangential forces. As shown in the Figure, forces are cyclic in nature, indicating a periodic material removal mechanism, with changes in value occurring rapidly resulting in the force data appearing tightly packed. Periodic spikes in temperature also occur, where it should be noted that the threshold for the pyrometer is 150°C. As expected, the duration of the axial incursion varies with time, decreasing progressively as the axial rate rises. Comparing across the incursion rates, the Fig. 10 also shows that axial forces rise in line with the incursion rate, with normal and tangential forces more stable. Temperatures appear to show no correlation with axial incursion rate, and are broadly similar in all cases investigated.

Fig. 11 shows the force and temperature measurement recorded with the fin segment. As shown, a similar pattern to as seen with the single fin
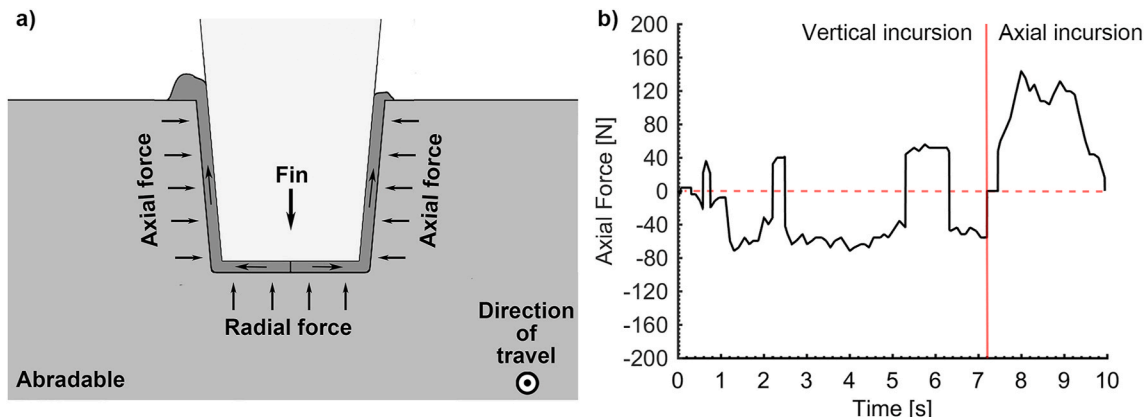

Fig. 9. schematic diagram of corresponding force in vertical incur and b) example axial force result (whole-ring fin, axial incursion speed 930μm/s)
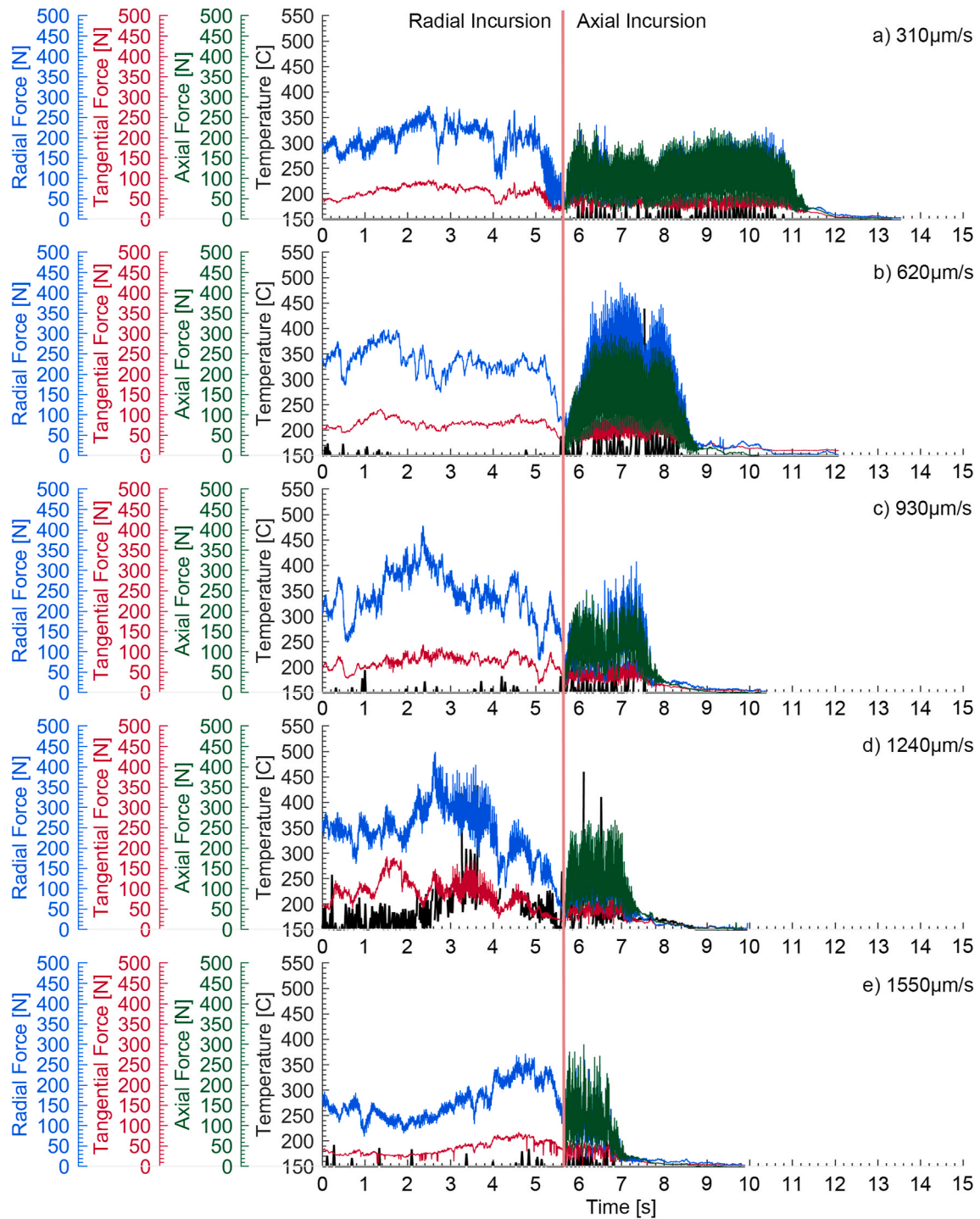
Fig. 10. In-situ force and temperature results, single discrete fin with axial incursion speed of a) 310µm/s, b) 620µm/s, c) 930µm/s, d) 1240µm/s and e) 1550µm/s

occurs, with higher radial and axial forces, followed by lower tangential forces. Overall magnitudes are also not dissimilar to the case of a single fin. However, whilst in the case of the single fin this ordering was clear, the tangential force is now closer to the other two components. Temperature spikes are also less significant in magnitude, although it does appear that temperatures above the 150°C threshold of the pyrometer are recorded more frequently. Finally, whilst for the single fin a correlation was established between axial force and incursion rate, whilst still the case, as for wear scar width, this correlation is reduced, with increased variation observed. Additionally high radial forces are recorded in Fig. 11b for the anomalous test performed at an axial incursion

rate of 620µm/s, aligning with observations with respect to the wear mechanism for this test.

Finally, Fig. 12 shows the force and temperature measurements from when four segments were joined together to form a continuous fin around the circumference of the disc. As shown, forces are generally lower than for the single fin and fin segment, and also with weak correlation to incursion rate. Variation between axial incursion conditions is now reduced, and it is noticeable that a reduced number of spikes in force and temperature occur. As has been the case for the other two fin geometries investigated, radial and axial forces are also once again the largest, with radial forces dominating more routinely in some cases.
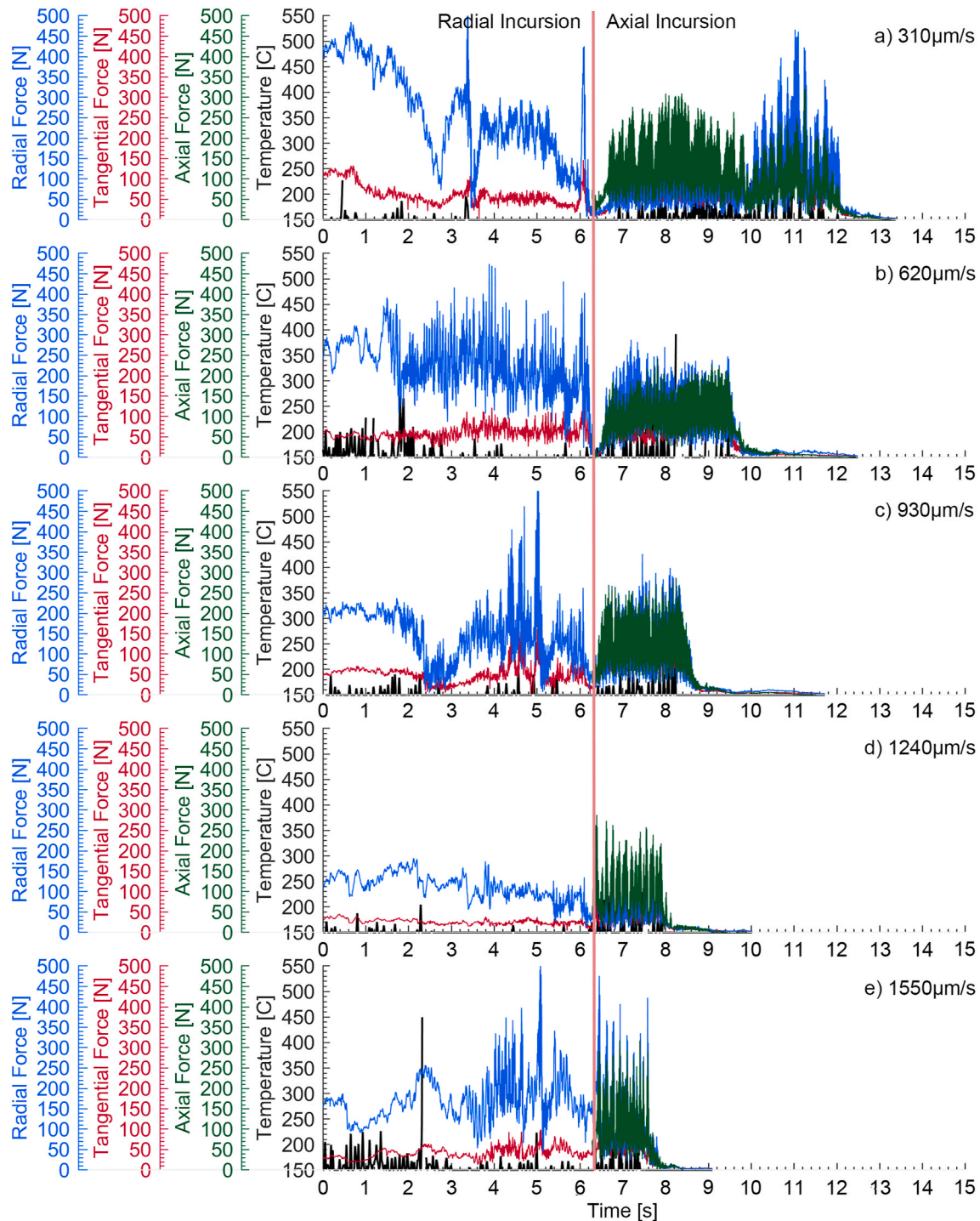
Fig. 11. In-situ force and temperature results, segment fin with axial incursion speed of a) 310μm/s, b) 620μm/s, c) 930μm/s, d) 1240μm/s and e) 1550μm/s

Fig. 13 shows the maximum and average forces for all of the tests performed, along with maximum temperature values. It should be noted that average temperatures are not included, as the measurement threshold for the pyrometer is 150°C, and recorded values frequently fall below this value making the average mis-leading. As such, only maximum values have been included. As has been detailed in the preceding section, radial and axial forces are the largest in the axial incursion event. The Figure also clearly highlights the limited correlation between forces and axial incursion rate for the fig segment and whole ring tests, with this particularly evident from the average force results. Whilst it is not surprising that axial forces are large given the

nature of the incursion, it is interesting to note radial forces are similar in value. However, given the angled nature of the fin, and the fact radial force has previously been linked to removal of material from the bottom of the worn groove in previous studies [1], this result is not surprising. Indeed, it suggests that extrusion and removal of material by the fin from this region is still a significant component of the wear mechanism. In particular, the result for the continuous fin supports this view, where the most rubbing occurs, given the continual nature of the contact.
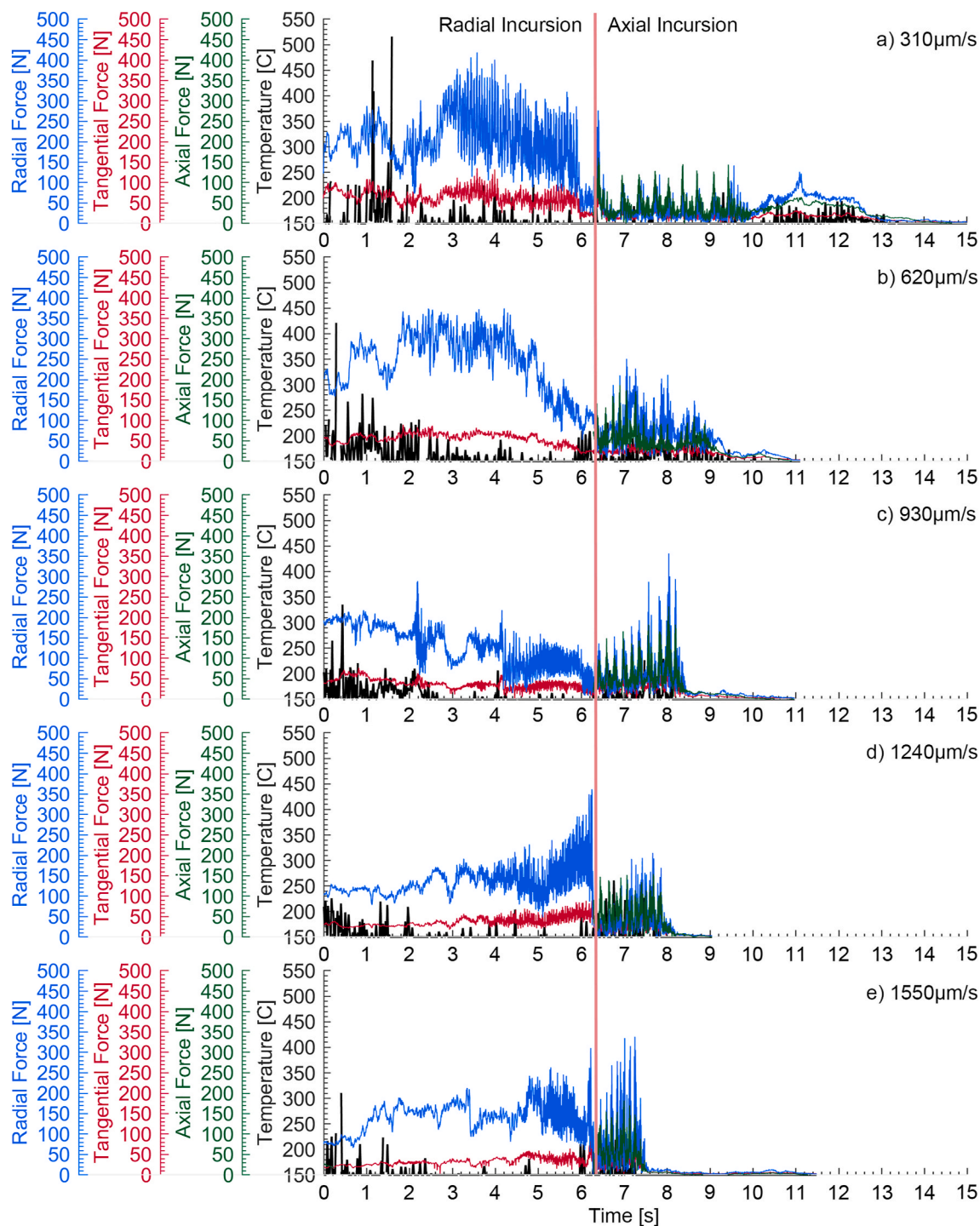
Fig. 12. In-situ force and temperature results, whole-ring fin with axial incursion speed of a) 310μm/s, b) 620μm/s, c) 930μm/s, d) 1240μm/s and e) 1550μm/s

3.3. Wear grooves surface microscope copies

Fig. 14 shows microscope images taken from the wear scars on the abradable sample. In the figures, the fin moves from left to right with rotation of the disc, and from the top to the bottom of the image during the axial incursion. As shown in the figures, for all fin samples investigated, at all axial incursion conditions, similar variability in the surface of the wear scar exists. In some instances, material appears fractured and well cut with light pitting, and in others is extruded to form a surface layer on the abradable. In this latter case, at the extreme the extruded material fractures and breaks away in chips(Figures 14a & g), with this

being similar to the mechanism identified for radial incursions by fins into an abradable [1]. However, as the scale of the pitting is relatively small, the overall change in the morphology of the wear scar is limited. As might be expected, the features identified vary in the axial direction, and are continuous along the line of fin rotation, with the exception being where the extruded surface fractures. It is also apparent that the wear mechanism varies within a given axial incursion event, with progression from well cut, to extrusion and smearing (with fracture in some cases), and back to good cutting of the abradable. These changes in wear mechanism are likely linked to adhesion of material to the fin, as well as removal of material from the worn groove, and will be discussed further
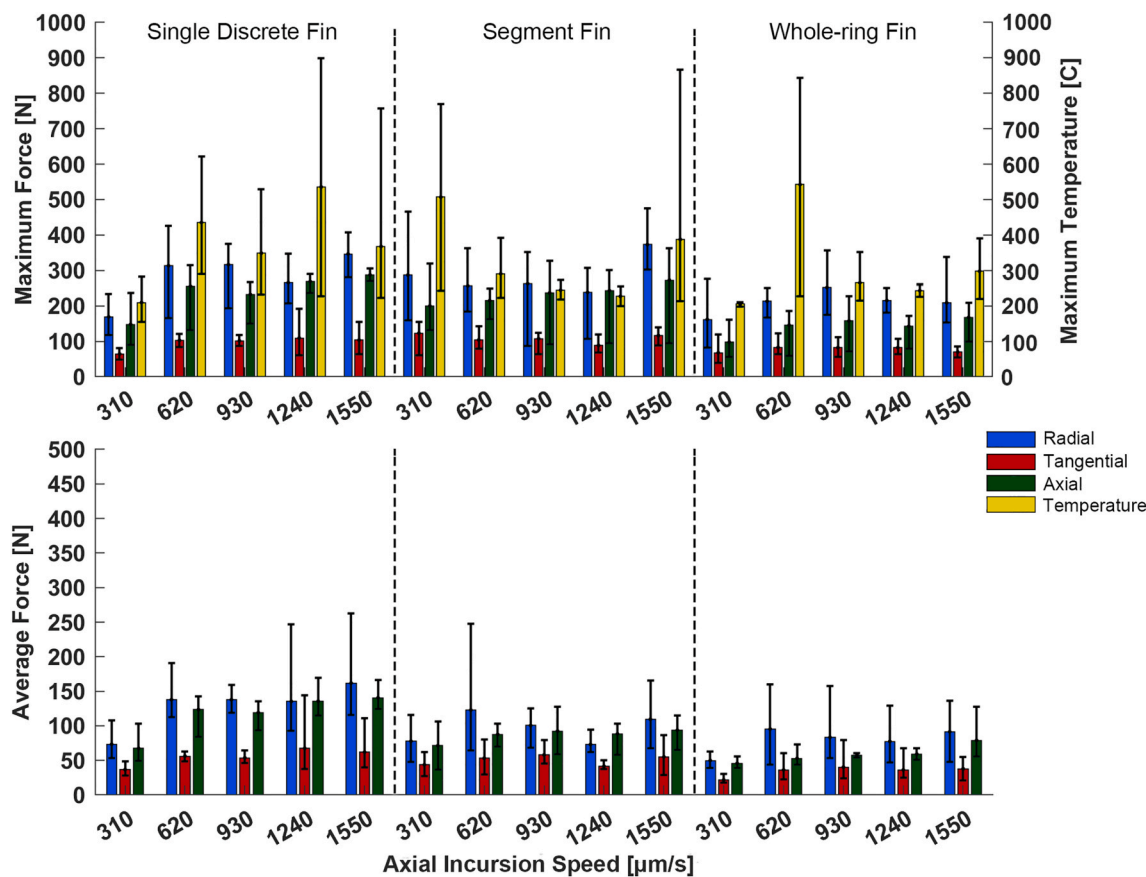
Fig. 13. a)maximum forces and temperatures and b) average forces for all axial incursion event

later.

Considering the individual fin geometries, Fig. 14a–e show the images of the wear scars from the single discrete fin. As the images of the wear scars in the figure show, the morphology of the wear scar indeed varies, with a gradual reduction in smearing as the axial incursion rate increases. Overall this is not very significant though, but it is interesting to note that it is linked with the gradual narrowing in the length of the wear scar previously noted, and clearly apparent in the images moving from left to right. Moving to the tests with the fin segments (Fig. 14f-j), the previously noted variation in wear scar morphology is evident, with little correlation between degree of cutting and axial incursion rate. Previously it was noted that significant adhesion occurred in the case of the test at an axial incursion rate of 620μm/s, with thermal damage also evident in the rub track. This issue is clearly visible in the image taken from this test (Figure 14g), where a long wear scar is present, and extrusion and fracture evident. However, it is also interesting to note that in the other cases where significant adhesion was evident (1240μm/s, Fig. 14i), a relatively well cut rub track is evident, and similar to the other tests for this fin type, where more moderate adhesion and over-cutting occurred. This suggests that the adhesion that led to the broadening of the wear scar happened early in the rub and then broke away, and a degree of recovery then took place. Finally, Fig. 14k–o show the images taken from the abradable samples tested with a continuous fin. As shown by the results for wear, force, and temperature, this fin type demonstrated the most consistent behaviour across all axial incursion conditions investigated, indeed the surface is generally well fractured, and whilst areas of extrusion do occur, these never progress to the point where fracture and peeling away of the surface occurs. It can also be seen from the images that the previous observation that the length of the wear track is similar in length at all axial incursion conditions is well supported.

3.4. In-situ abradable surface image capture

The observations presented so far, suggest that during axial incursions material is able to successfully exit the contact zone. Whilst clear some level of adhesion to the fins exists, with corresponding increases in force and temperature, along with smearing and fracture of the run track, an extreme wear evident does not take place. Comparing back to tests with fins incurring radial into an abradable [1], this suggests material is extruded out of the contact much like occurs at higher incursion rates, as opposed to the smearing and fracture seen when the incursion rate is lower. As has been demonstrated previously [1], the use of stroboscopic imaging focused on material removal from the rub track, gives good insight into this mechanism.

Fig. 15 shows the images captured with the side camera during the test, where the time stamps shown in red in the right corner of each frame, indicate the point in the test from which the image is taken. It should be noted that due to sparks occurring during the rubs, the image quality is variable, and in some cases it is difficult to post-process them as they are overexposed. As such, sequences of images at three different incursion rates have been selected for each fin type investigated, with the aim of demonstrating material removal from the contact. In each case, images are spaced to show how extruded material first develops, grows in size, and ultimately fractures off. As shown by the images, abradable material is generally pushed up the side of the worn groove during the incursion event. Given the fins tapered geometry and the fact the axial incursion rates investigated are relatively high, this should to a degree be expected, particularly considering extrusion was evident in previous studies with single fins at high incursion rates [1,2]. It is also evident that the level of extrusion, period of growth, and point of break off is variable. However, given the limited data set and issues with over exposure, whilst tempting, it is not possible to make firm conclusions with respect to how this varies with fin type or axial incursion rate.
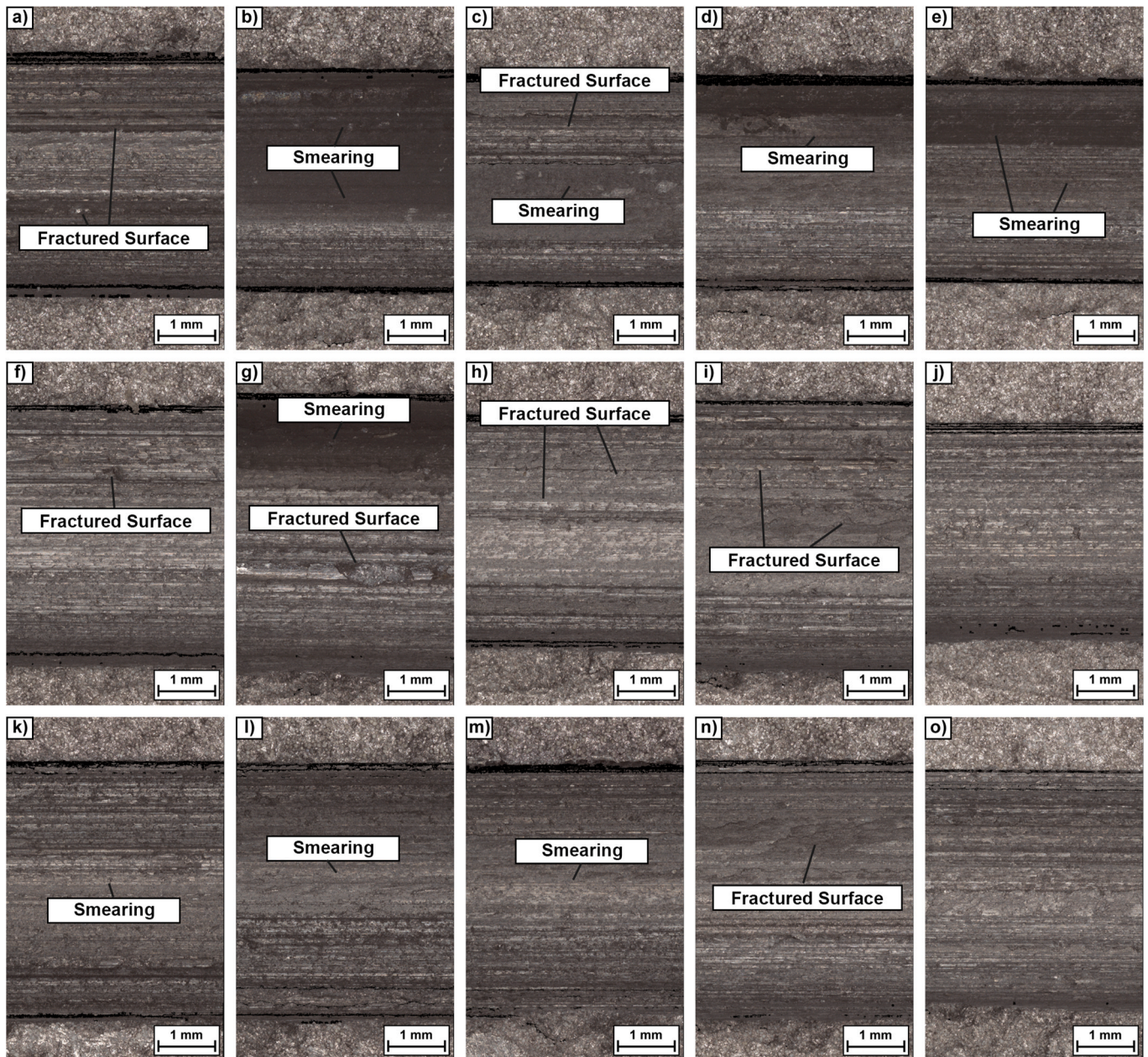
Fig. 14. Wear groove microscopies for all test, single discrete fin with axial incursion speed of a) 310μm/s, b) 620μm/s, c) 930μm/s, d) 1240μm/s and e) 1550μm/s; segment fin with axial incursion speed of f) 310μm/s, g) 620μm/s, h) 930μm/s, i) 1240μm/s and j) 1550μm/s and whole-ring fin with axial incursion speed of k) 310μm/s, l) 620μm/s, m) 930μm/s, n) 1240μm/s and o) 1550μm/s;

4. Discussion

From the force and temperature results, alongside imaging of the worn samples and material removal during the test, insight can be gained into the material removal mechanism during the axial incursion event. Following this, the influence of incursion rate and fin geometry will also be considered.

4.1. Abradable material removal mechanism in axial movement

As highlighted from the images taken of material removal during the axial incursion event, material is extruded out of the contact, moving up the interface between the fin and abradable on the side on which the incursion is taking place, before eventually fracturing off when a critical length is reached. This process is shown schematically in Steps 1 and 2 in Fig. 16, where how the angular nature of the fin promotes this

mechanism is highlighted. From inspecting the fin samples post-test, adhesion of abradable material to the fin was also evident (Fig. 16, Steps 3 and 4), with this leading to overcutting (extension of the groove length in the axial direction). This is a similar result to that seen for low rate vertical incursions with fins [1], but in this case occurred in the majority of conditions tested. However, considering the nature of the contact in the axial contact, and the fact the abradable is now directly pressed against the side of the fin, it is reasonable that adhesion is more prevalent. It is also interesting to note that for the discrete fin that adehesion occurs at its extremities, with this likely due edge effects, as well as local deformation and non-perfect rotation of the test sample. Comparing more generally to compressor blade – abradable liner contacts, the volume of adhesion, and indeed the rate it occurred at, was found to be a function of incursion rate, and whether this is the case for fins will be investigated further in the following section. Considering the variation seen in the force results, this process also appears to be highly
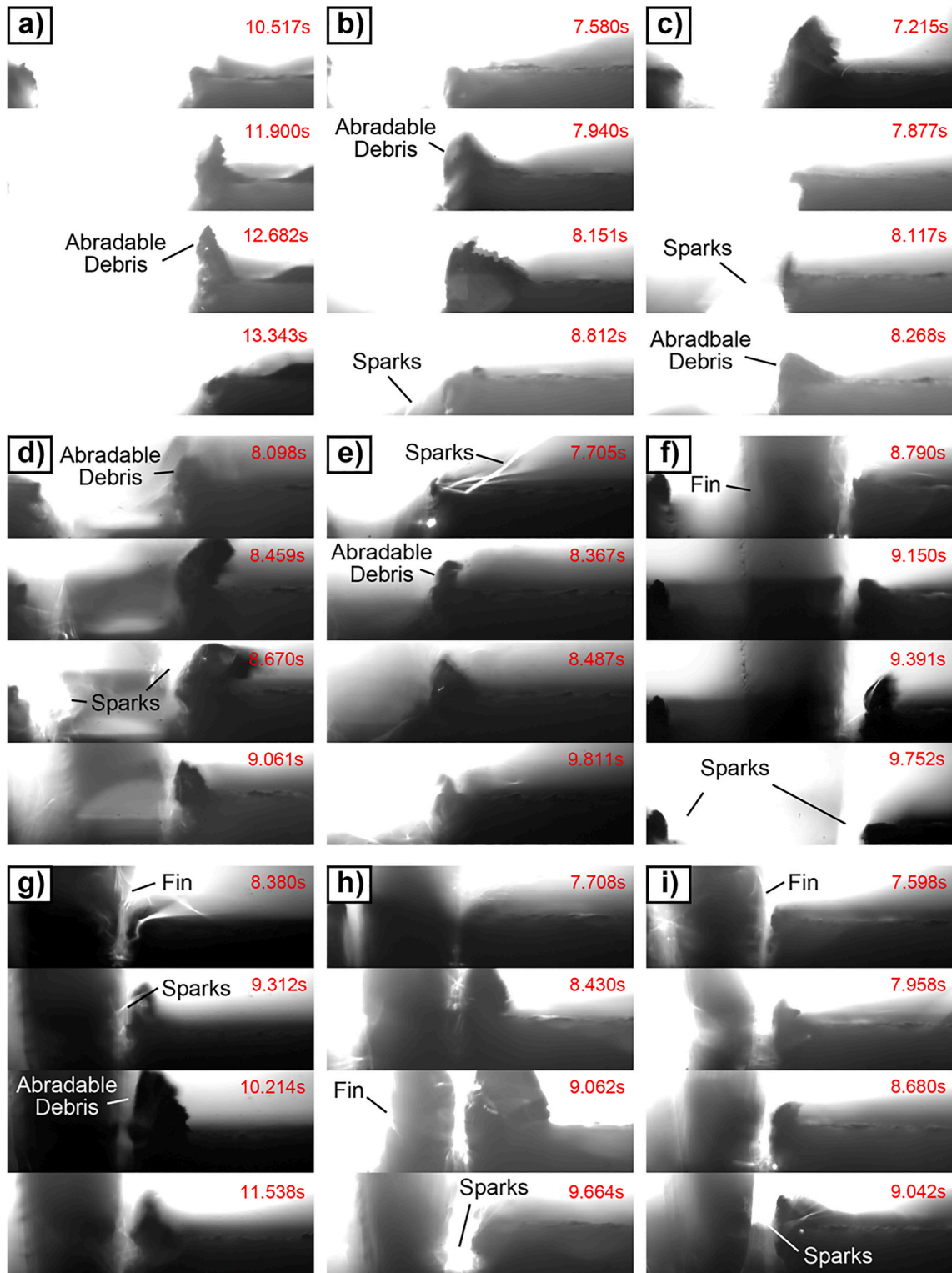
Fig. 15. Part of side camera images from test, single discrete fin with axial incursion speed of a) 310μm/s, b) 930μm/s and c) 1550μm/s; segment fin with axial incursion speed of d) 620μm/s, e) 930μm/s and f) 1550μm/s; and whole-ring fin with axial incursion speed of g) 310μm/s, h) 930μm/s and i) 1240μm/s

transient, and subject to a significant rate of change within a test.

Observing the troughs of the wear scar created on the abradable, alongside the force and temperature measurements, gives further insight into the removal mechanism, and suggest that the material removal mechanism is not as simple as suggested, and indeed is likely to consist of abrasive wear, extrusion (creep), as well as compression and fracture. Given the steep nature of the fin, it might be expected that the axial

component of the measured force dominates, and the radial component is significantly smaller. However, as shown by the force results, vertical forces are still significant, and at times are of a similar scale to those measured in the axial direction. Indeed, peaks in these radial forces are found to correlate with spikes in temperature, and smearing of material in the base of the rub track. Much like in the case of a radial incursion [1], these observations suggest that some material fails to extrude,
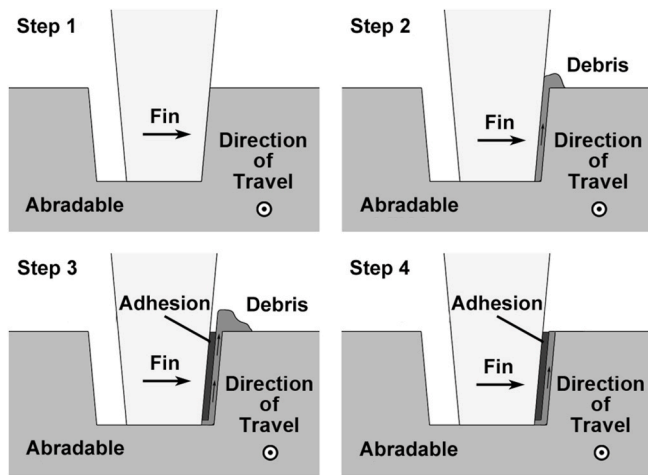
Fig. 16. Schematic diagram of abradable material removal mechanism with axial movement

becoming smeared on the surface of the rub track, before eventually being released via fracture. Similarly, as highlighted by fracture in the abradable wear track, that as well as extruding up the face of the fin, some material becomes trapped under the fin during the axial incursion, leading to the aforementioned compaction and build-up of force and temperature prior to release. This is particularly evident for the test with the pair of fin segments at an axial incursion speed of 620μm/s, where clearly an extreme version of this scenario occurs. Finally, abrasive wear is likely to occur as the blade rubs against the abradable, with damage observed on both the fin and abradable sample indicative of this.

4.2. Effect of incursion speed & fin type

As noted, in the case of either blades or fins incurring vertically into abradable systems, the wear mechanisms present tend to be a function of incursion rate [1,14,15]. In this case, the mechanism is one of adhesion of material to the fin, followed by fracture. Considering the results for the single fin shown in Fig. 8a, the level of adhesion does appear to depend on axial incursion rate, with the most overcutting and presumably highest levels of adhesion occurring at the lowest axial rate. This result aligns well with those seen for blades incurring aluminium based abradables where, as the incursion rate increases, adhesion reduces and cutting occurs. However, given the blunt nature of the fin contact, a transition to cutting is less likely to occur, and the reduction in adhesion is more likely due to another factor. The continuous progression of the axial stage, combined with the short arc length of the fin, means that the abradable advances significantly while the fin is out of contact. This results in a significant entry shock, as the fin overlaps the groove in the abradable on a strike by strike basis, with a degree of cutting likely to occur in this process. As the incursion rate increases, so does the overlap, and given its blunt nature, as do the forces associated with it. Consequently, it becomes more likely adhered material from the rubbing component of the contact is removed, and as such adhesion decreases with axial incursion rate.

Considering the results for the segments used in a pair (Fig. 8b), and the whole ring (Fig. 8c) supports this view. For the segments used as a pair, adhesion is on average higher, shows reduced correlation with axial incursion rate, and is prone to variability. Given this fin type spends approximately half of the time rubbing the abradable, compared to a very small time period for the single fin, it is unsurprising adhesion increased. However, as non-contact still occurs for half of the revolution (in two 90 degree arcs), an abrupt entry to contact still persists, and some correlation between adhesion level and axial incursion rate is seen. That said, how vulnerable the adhesions are to removal will be dependent on their proximity to the leading edge, with this presumably

leading to the variations seen in the results seen for overcutting. In turn this leads to more smearing on the rub track surface. Moving to the whole ring, adhesions are reduced when compared to the paired segments, but still higher than that seen for the single fin. Interestingly, correlation with axial incursion rate is further reduced, and variability is also decreased. Going back to a previous study [6] on the role of fin geometry in fin – abradable interactions, it was concluded that whilst rubbing increased for a whole ring fin, leading to a greater thermal input, the ability to remove heat from the contact was also enhanced, due to the continuous nature of the contact. As such, it was shown to develop lower temperatures in the contact than for a pair of fin segments, where significant rubbing also occurred [6]. This result goes some way to explaining the trends seen in this study, where overall adhesion is lower for the whole ring, driven by lower temperatures in the contact. This combined with the continuous nature of the contact, means the adhesion is also both more stable and less dependent on incursion rate, resulting in the lack of variability and strong dependence on incursion rate shown. That said, spikes in temperature do still occur when adhesions build, and it would be interesting as an area of future work to both fully thermally model the contact, and also measure it using a thermal camera.

4.3. Abradable material removal efficiency

In the previous section, the role of fin geometry was considered, where the discrete nature of the contact was observed to have an impact on the ability of material to adhere to the fin. Specifically, it was identified that for the single fin, axial progression of the abradable occurred whilst the fin was out of contact, resulting in significant overlap between the fin and abradable as contact began, and break off of adhered material. Conversely for the whole ring, a continually rubbing contact occurs. Given these differences in interaction between the abradable and different fin geometries, it is of interest to consider how they impact the efficiency of material removal. One way to do this, previously employed for abradable materials [1] and adapted from machining science [16], is to consider the total energy consumed by the extrusion process. Given the axial incursion by the fin, this consists of work done in the axial and tangential directions, calculated using the measured forces combined with the rub length and incursion depth, and is expressed as follows:

$$E_{total} = W_f + W_i = F_x \times L + F_y \times id \tag{1}$$

where F_x is the average tangential force, L is total rub length, F_y is the average axial force, and id is the incursion depth. As shown, the Equation contains two terms, representing the energy consumed during the rub. The first term is frictional work which is mainly represented by the measured tangential force, and the second part is work done when directly removing material, calculated from the axial force.

Fig. 17 shows the total energy consumed in each case, where on average for a given incursion rate, the energy required to remove the material is lowest for the single fin and highest for the whole ring. Although it should be noted that values for the two cases where fin segments are used, either in a pair or to form a whole ring, have similar values. This analysis is included given the different fin contacts considered, in order to explore where they have fundamental influenced the efficiency of material removal. Going back to machining theory [17] this is likely due to the fact for the single fin a degree of cutting occurs, due to the progression of the abradable when the fin is not in contact, and rubbing dominating for the two tests with fin segments, with a slightly more extreme case for the whole ring. Looking across incursion rates, as previously noted when discussing wear mechanics, a degree of change does occur for each fin type, with an increase in incursion rate resulting in a reduction in energy consumed. However, as was also noted previously, this trend is more significant for the single fin. This result is significantly different to those of radial incursions with fins, where a pronounced improvement in efficiency of cut with incursion rate was
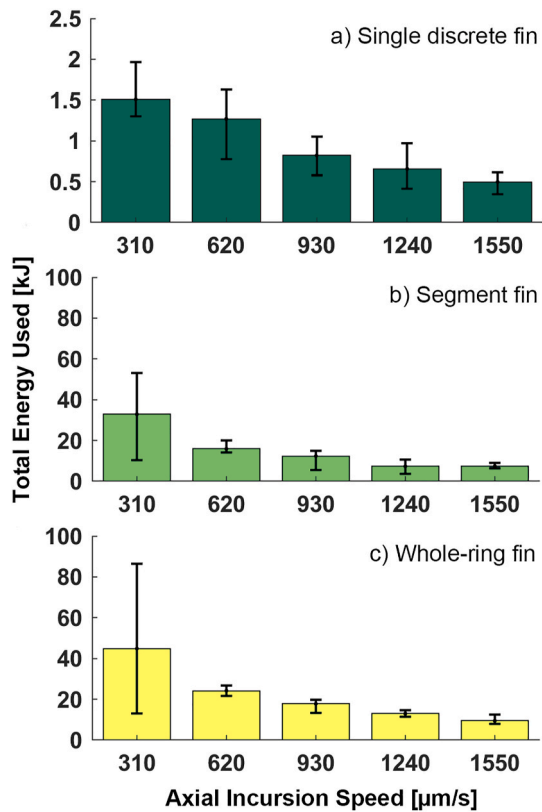
Fig. 17. Bar charts of estimate total energy used for tests with a) single discrete fin (40x smaller y-axis scale), b) segment fin and c) whole-ring fin

observed. For example, for radial incursions with a single fin on the same abradable as investigated in this study, in order to remove 2mm of material, 20kJ of energy was required if this was done at 0.02μm/pass, dropping to 1kJ in the case of 2μm/pass [1]. Overall, this highlights that whilst extrusion based, the wear mechanism for axial incursions is different, with an increase in rate not significantly promoting improvements in material removal.

5. Conclusions

This study investigated the abradable removal mechanism for axial fin rubs, considering both the influence of incursion speed as well as fin profile on the mechanism. From the work the following conclusions can be made:

- In a similar manner to vertical incursions, the abradable material is mainly removed by an extrusion process, with adhesion of abradable material to the fin also occurring.
- Adhesion of material to the fin resulted in overcutting, and was found to reduce for a single fin, as axial incursion rate increased.
- Adhesion was greater for the fin segments, either when used as a pair of whole ring, with reduced reduction with incursion rate.
- Moving from a single fin, two more continuous contacts, promoted increased rubbing, leading to increased thermal effects, seen both in aforementioned adhesion, and in smearing of abradable material in the worn groove.
- Overall, the angular nature of the fin promotes extrusion of material, however, it is important to consider the specific nature of the contact and rate at which it occurs when contextualising results, given the influence of these two variables demonstrated.

Authorship contributions

Please indicate the specific contributions made by each author (list the authors' initials followed by their surnames, e.g., Y.L. Cheung). The name of each author must appear at least once in each of the three categories below. Category 1 Conception and design of study:Conceptualization: B. Zhang, M. Marshall; acquisition of data: B. Zhang; analysis and/or interpretation of data: B. Zhang. Category 2 Drafting the manuscript: B. Zhang, M. Marshall, R. Lewis; revising the manuscript critically for important intellectual content: B. Zhang, M. Marshall. Category 3Approval of the version of the manuscript to be published (the names of all authors must be listed): B. Zhang, M. Marshall, R. Lewis.

Declaration of competing interest

The authors declare that they have no known competing financial interests or personal relationships that could have appeared to influence the work reported in this paper.

Data availability

Data will be made available on request.

Reference

[1] B. Zhang, M. Marshall, Investigating material removal mechanism of Al-Si base abradable coating in labyrinth seal system, Wear 426–427 (2019) 239–249, https://doi.org/10.1016/j.wear.2019.01.034 (A).

[2] C. Delebarre, V. Wagne, J.Y. Paris, G. Dessein, J. Denape, J. Gurt-Santanach, Tribological characterization of a labyrinth-abradable interaction in aturbo engine application, Wear 370-371 (2017) 29–38, https://doi.org/10.1016/j.wear.2016.11.007.

[3] N. Zhang, H. Xuan, X. Guo, C. Guan, W. Hong, Investigation of high-speed rubbing behavior of labyrinth-honeycomb seal for turbine engine application, Journal of Zhejiang University - Science A (Applied Physics & Engineering) 17 (12) (2016) 947–960, https://doi.org/10.1631/jzus.A1600367.

[4] T. Pychynski, C. Höfler, H. Bauer, Experimental study on the friction contact between a labyrinth seal fin and a honeycomb Stator, Journal of Engineering for Gas Turbines and Power 138 (2016) 9, https://doi.org/10.1115/1.4031791, 062501-1-062501.

[5] B. Lu, X. Ma, C. Wu, H. Xuan, W. Hong, The Wear of Seal Fins during High-Speed Rub between Labyrinth Seal Fins and Honeycomb Stators at Different Incursion Rates, Materials 14 (2021) 979, https://doi.org/10.3390/ma14040979.

[6] B. Zhang, M. Marshall, R. Lewis, An Investigation into the Role of Specimen Geometry when Undertaking Tribological Testing on Seal Fin Components, Proc IMechE Part C: J Mechanical Engineering Science (2021), https://doi.org/10.1177/09544062211025058.

[7] J. Stringer, M. Marshall, High speed wear testing of an abradable coating, Wear 294-295 (2012) 257–263, https://doi.org/10.1016/j.wear.2012.07.009.

[8] N. Fois, J. Stringer, J.M. Marshall, Adhesive transfer in aero-engine abradable linings contact, Wear 304 (No. 1-2) (2013) 202–210, https://doi.org/10.1016/j.wear.2013.04.033. Wear 304 (2013) 202–210.

[9] Oerlikon Metco, Material Product Data Sheet - Aluminum Silicon Polymer Thermal Spray Powders, 2016.

[10] Sulzer Metco®. Technical Bulletin #10-141. 2000.

[11] ASM Material Data Sheet - AISI Type 304 Stainless Steel, Asm.matweb.com, 2019. Apr, http://asm.matweb.com/search/SpecificMaterial.asp?bassnum=mq304a.

[12] ASM Material Data Sheet - Titanium Ti-6Al-4V (Grade 5), Asm.matweb.com, 2019. Apr, http://asm.matweb.com/search/SpecificMaterial.asp?bassnum=mtp641.

[14] W. Xue, S. Gao, D. Duan, J. Zhang, Y. Liu, S. Li, Effects of blade material characteristics on the high-speed rubbing behavior between Al-hBN abradable seal coatings and blades, Wear 410-411 (2018) 25–33, https://doi.org/10.1016/j.wear.2018.06.003.

[15] M. Thévenot, V. Wagner, J.-Y. Parisa, G. Dessein, J. Denape, M. Harzallah, A. Brunet, T. Chantrait, Thermomechanical phenomena and wear flow mechanisms during high speed contact of abradable materials, Wear 426-427 (2019) 1102–1109, https://doi.org/10.1016/j.wear.2019.01.094.

[16] V. Chiles, S. Black, A. Lissaman, S. Martin. Principles of Engineering Manufacture (3rd Edition). ISBN: 9780340631959.

[17] D. Stephenson, J. Agapiou, Metal cutting theory and practice - Chapter 6, 3rd Edition, CRC, Taylor & Francis group, Boca Raton, 2016, pp. 393–439.